HHS Public Access

Author manuscript

ACS Sens. Author manuscript; available in PMC 2021 May 22.

Published in final edited form as:

ACS Sens. 2020 May 22; 5(5): 1419–1426. doi:10.1021/acssensors.0c00307.

A fluorescent and surface-enhanced Raman spectroscopic dual-modal aptasensor for sensitive detection of cyanotoxins

Ming Li[†,‡,*], **Hangduo Lin**[†,#], **Santosh Kumar Paidi**[‡,#], **Nicolas Mesyngier**[‖,#], **Sarah Preheim**[⊥], **Ishan Barman**[‡,§,※,*]

[†]School of Materials Science and Engineering, Central South University, Changsha, Hunan 410083, China

[‡]Department of Mechanical Engineering, The Johns Hopkins University, Baltimore, Maryland 21218, USA

[‖]Department of Engineering Science and Mechanics, The Pennsylvania State University, University Park, Pennsylvania 16802, USA

[⊥]Department of Environmental Health and Engineering, The Johns Hopkins University, Baltimore, Maryland 21218, USA

[§]Department of Oncology, The Johns Hopkins University School of Medicine, Baltimore, Maryland 21287, USA

[※]The Russell H. Morgan Department of Radiology and Radiological Science, The Johns Hopkins University School of Medicine, Baltimore, Maryland, 21287, USA

Abstract

The ability to detect trace analytes without necessitating solid surface attachment or complicated processing steps would facilitate the translation of sensors for monitoring environmental toxins in the field. To address a critical unmet need in fresh water ecology, we have developed a dual-modal aptamer-based biosensor (aptasensor), featuring fluorescence and surface-enhanced Raman spectroscopy (SERS), for sensitive and selective detection of hepatotoxin microcystin-LR (MC-LR). The rational sensor design is based on the high affinity of the cyanine (Cy3) dye-modified complementary DNA (Cy3-cDNA) strand toward the plasmonic gold nanostars (GNSs) in comparison to the Cy3-cDNA/aptamer duplex. The preferential binding of MC-LR toward the MC-LR specific aptamer triggers the dissociation of Cy3-cDNA/aptamer duplexes, which switches the Cy3's fluorescence "off" and SERS "on" due to the proximity of Cy3 dye to the GNS

[*]**Corresponding Author** Ming Li, liming0823@csu.edu.com and liming0823@gmail.com, Ishan Barman, ibarman@jhu.edu.
[#]These authors have made equal contributions

The authors declare no competing financial interest.

Supporting Information.

This Supporting Information is available free of charge via the Internet at http://pubs.acs.org.

Absorption spectra and representative TEM image of Cy3-cDNA-GNS conjugates of GNSs and Cy3-cDNA-GNS conjugates; Schematic of preparation of Cy3-cDNA-GNS conjugates and Cy3-cDNA/aptamer-GNS conjugates; Details of quantification of the Cy3-cDNA coverage on the gold nanostar surface; UV-vis absorption spectra of Cy3-DNA solutions before and after the GNS was added; Spontaneous Raman and SERS spectra of Cy3-cDNA and physically mixed Cy3-cDNA with GNSs; UV-vis absorption and fluorescence emission spectra of Cy3-cDNA, and steady-state fluorescence emission spectra of Cy3-cDNA/aptamer-GNS conjugates upon addition of various concentrations of MC-LR; SERS spectra of Cy3 in the aptasensor as a function of the MC-LR concentration; SERS spectra and real-time fluorescence response of real water samples

surface. Both fluorescence and SERS intensities are observed to vary linearly with the MC-LR concentration over the range of investigation. We have achieved high sensitivity and excellent specificity with the aptasensor toward MC-LR, which can be attributed to the fluorescence quenching effect, significant SERS enhancement by the GNSs and the high affinity of the aptamer toward the MC-LR analytes. We further demonstrate the applicability of the present aptasensor for detection of MC-LR in a diverse set of real water samples with high accuracy and excellent reproducibility. With further refinement, we believe that the aptamer-driven complementary assembly of the SERS and fluorescence sensing constructs can be applied for rapid, multiplexed and robust measurements of environmental toxins in the field.

Keywords

fluorescence; surface-enhanced Raman spectroscopy; dual-modality detection; aptasensor; microcystins

Development of deployable sensing technologies for the detection of environmental toxins such as microcystins would have significant environmental and health benefits.[1–7] Microcystin-LR (MC-LR), one of the common cyanotoxins present in freshwater, originates from blue-green algae and can cause rapid liver failure. Prolonged exposure at low concentrations of MC-LR in drinking water has been reported to result in liver cancer because of the accumulative damage.[8] The World Health Organization (WHO) suggests a provisional upper limit of 1.0 μg/L for MC-LR in drinking water.[9] Several quantitative methods have been developed for microcystin detection including high-performance liquid chromatography (HPLC), liquid chromatography-mass spectroscopy (LC-MS), enzyme-linked immunosorbent assay (ELISA), mouse bioassays, and protein phosphatase inhibition assays (PPIA).[8,10] Despite their advantages in some aspects, these techniques require extensive equipment, operator expertise, complex sample preparation, and (or) long analysis time. The lack of sensitivity and selectivity in some of the simpler methods limits their capability of detecting MC-LR at very low concentrations. In addition, the high cost, poor stability and strict low-temperature storage conditions of antibodies make antibody-based immunoassays challenging for practical field applications.[10]

To meet this need, our sensor design involves aptamer-driven assembly of surface-enhanced Raman spectroscopy (SERS) and fluorescence sensing constructs, where the signal enhancement/reduction arises from the relative proximity of the reporter molecule to the intense localized plasmon fields created by the nanoparticles.[11–17] Noble metallic nanostructures have played a key role in fluorescence resonance energy transfer (FRET) sensors owing to their efficient fluorescence quenching ability when the fluorophore is proximal to the nanoparticle surface.[18,19] However, at a distance of a few nanometers (5–20 nm) from the metal surface, fluorescence has been shown to be greatly enhanced because of the plasmon resonance effect.[20,21] Also, the giant electromagnetic field enhancement has been exploited to develop SERS sensing platforms that enable single-molecule detection sensitivity with molecular specificity and powerful multiplex detection capability, attributed to those narrow Raman signatures achievable with a single excitation source.[22–27] The SERS

enhancement is usually distance-dependent and decreases with distance from the metal surface, in stark contrast to the plasmon-enhanced fluorescence.[9,14]

Due to the shared origins of plasmon resonance effects, opportunities for integration of SERS and fluorescence into a single nanoparticle-based probe have been explored to improve measurement precision and robustness while circumventing modality-specific limitations.[28–34] Thus, fusion of different sensing approaches could also produce a new multi-modal paradigm for environmental monitoring and enable the improvement of sensing performance with additional information unachievable by the individual technologies alone. The potential of such an integrated sensing construct obtained by controlling SERS and plasmon-enhanced fluorescence, however, has been surprisingly underappreciated.

In this work, we present an aptamer-based biosensor (aptasensor) that allows sensitive dual-modal detection of microcystin-LR (MC-LR) by harnessing real-time fluorescence and SERS measurements. We used the MC-LR specific aptamer as the recognition element in our probe design because of its high chemical and thermal stability, low cost and easy functionalization. The underlying mechanism of this dual-modal sensing platform is the differential affinity of single-stranded DNA (ssDNA) and double-stranded DNA (dsDNA) with the gold surface.[35,36] The complementary ssDNA labeled with the Cy3 dye (Cy3-cDNA) is conjugated via a thiol group onto the plasmonic gold nanostars (GNSs) to exhibit an intense (and tunable) plasmon resonance band in the visible-near infrared (NIR) region.[37] The hybridization of cDNAs with the MC-LR specific aptamer forms the Cy3-cDNA/aptamer duplex rigidly sitting on the GNS. The Cy3-cDNA single strand sticks to and folds onto the GNS surface due to its high flexibility and high affinity of exposed bases towards gold, while the rigid Cy3-cDNA/aptamer duplex does not coil around the GNS surface. Thus, pronounced, but opposite, changes in fluorescence and SERS intensities are observed following the addition of samples containing MC-LR. Crucially, the quantitative response of both fluorescence and SERS intensities as a function of the MC-LR concentration underscores its ability to accurately determine the microcystin content in diverse environments. Furthermore, the excellent specificity of this sensor is demonstrated by performing measurements with other microcystin analogues, such as MC-RR and MC-YR, which differ by just one functional group. The promising results of this pilot study pave the way for the integration of developed dual-modal aptasensor with emerging droplet microfluidic platforms to enable field translation for continuous substrate-free monitoring of toxins in freshwater ecosystems.

RESULTS AND DISCUSSION

GNSs possess multiple sharp protruding tips as built-in “hot spots”, which offer excellent fluorescence and SERS enhancement.[37,38] Here, GNSs with a plasmon resonance wavelength of 687 nm, prepared by controlling the Au seed/Au^{3+} ratio, are adopted because of their high electric field ($|E|^2/|E_0|^2$) enhancement of *ca.* four orders of magnitude (Figures 1 and S1A). Cy3-cDNAs are conjugated onto the GNS surface leveraging the strong Au-S interaction to prepare the Cy3-cDNA-GNS conjugates, in which the Cy3 dye functions as the fluorophore and Raman reporter for the fluorescent-SERS dual-modal detection (Figure S2). Negligible changes are observed in the absorption spectra of GNSs after conjugation

with the thiolated Cy3-cDNA (Figure S1A). The lack of new plasmon resonance bands in Cy3-cDNA-GNS conjugates indicates negligible interaction between the Cy3-cDNA single strands and the neighbouring GNSs. No aggregation is observed in the solution of Cy3-cDNA-GNS conjugates due to the negatively charged DNA single strands.[35] The coverage of cDNA is estimated to be *ca.* 4862 cDNA strand per GNS (Figure S3). Upon the addition of MC-LR-specific aptamers, the Cy3-cDNA/aptamer duplexes on the GNS are formed due to the hybridization of Cy3-cDNA with the aptamer.

The central idea for our aptasensor design is that Cy3-cDNA and Cy3-cDNA/aptamer duplexes have differential affinity toward the gold surface. Specifically, Cy3-cDNA of a single strand structure has exposed bases so that it sticks and folds on the GNS surface due to the high affinity between the bases of Cy3-cDNA and the GNS. In contrast, the Cy3-cDNA/aptamer duplex does not fully expose its bases and always presents the negatively charged phosphate backbone outwards to prevent coiling around the gold surface.[10,35] Thus, in the absence of MC-LR, the rigid duplex structure keeps the Cy3 dye *ca.* 13 nm away from the GNS surface due to which strong fluorescence and weak SERS signals are observed. In the presence of MC-LR, the strong interaction of the aptamer with the Arg and Leu of MC-LR contributes to the high affinity between MC-LR analytes and aptamers; the stable MC-LR-aptamer complexes are consequently formed accompanied by the dissociation of the Cy3-cDNA/aptamer duplexes.[39] As a result, the Cy3-cDNA is flexible enough to stick to the GNS surface leading to the fluorescence quenching and SERS enhancement.

To make the detection possible at room temperature, we first optimize the NaCl concentration by measuring the melting profiles of the Cy3-cDNA/aptamer-GNS conjugates at varying NaCl concentrations.[40] The absorbance at 260 nm is monitored as a function of temperature (Figure 2A). It can be seen that the melting temperatures are 47, 53 and 57 ^{o}C for 50, 100 and 150 mM NaCl, respectively; the absorbance starts to increase at 29 ^{o}C (close to room temperature) when the NaCl concentration is 50 mM. Therefore, we choose to use 50 mM NaCl concentration for the ensuing experiments in this work. The preferential binding of Cy3-cDNA to the GNS surface is confirmed by changes of fluorescence and SERS intensities before and after the dissociation of the Cy3-cDNA/aptamer duplexes on the GNS (Figure 2B). The Cy3-cDNA-GNS conjugates exhibit a fluorescence peak at 565 nm, consistent with that of the Cy3-cDNA alone; however, the fluorescence intensity increases by 17-fold after forming the Cy3-cDNA/aptamer duplexes on the GNS. Considering the ~13 nm distance away from the Cy3 dye to the GNS surface, we attribute the fluorescence recovery to the plasmonic enhancement of fluorescence by the GNSs.[20,41] While we do not find the spontaneous Raman bands of the Cy3 dye in the Cy3-cDNA even at a high laser power of 60 mW, we observe Cy3 dye-associated SERS bands at approximately 924, 1125, 1191, 1236, 1273, 1394, 1471 and 1587 cm^{-1} for the low laser power of 5 mW when the Cy3-cDNA is mixed with GNS colloids (Figures 2B and S4). The SERS bands at 924, 1191, 1273, 1394 and 1471 cm^{-1} are assigned to the C-H out-of-plane bending mode, the C-H in-plane bending mode, the motion of -CH_2- attached to the aromatic moiety, the CH_3 symmetric deformation, and the C=C stretching vibration in the benzene ring, respectively. Detailed assignments of the SERS bands of Cy3-cDNA-GNS conjugates can be found in Table 1.[42,43]

In the case of Cy3-cDNA-GNS conjugates, the Cy3-cDNA sticks to the GNS surface so that the Raman bands of Cy3 dye experience significant electromagnetic enhancement to produce strong SERS signals. Expectedly, the Cy3-cDNA/aptamer-GNS conjugates have weaker SERS intensities. All of these results indicate that Cy3-cDNA-GNS conjugates and Cy3-cDNA/aptamer-GNS conjugates exhibit distinct fluorescence and SERS intensity of Cy3 due to their differential affinity towards the GNS surface and thus paving the way for dual-modal quantitative detection of MC-LR.[35]

Next, we evaluate the fluorescence and SERS response in the presence of MC-LR. The response kinetics of the aptasensor for MC-LR reveal that the fluorescence response ((F_0-F)/F_0) gradually increases with time and finally reaches saturation within 120 s at 50 μg/L MC-LR and 180 s at 20 μg/L (Figure 3A). The steady-state fluorescence intensity change is linearly proportional to the concentration of MC-LR over a range from 0.1 μg/L to 50 μg/L (Figures 3A and S5). Based on the averaged values of three repeat measurements, the calibration curve is linearly fitted to be y=0.01741•x (R^2=0.998). Similarly, the SERS response of the aptasensor toward MC-LR is examined with various concentrations of MC-LR (Figures 3B and S6). It can be clearly seen that the SERS intensity increases with the increase of MC-LR concentration. The calibration curve is linearly fitted to be y=1.315•x +4.297 (R^2=0.984). The limit of detection (LOD) is determined to be 0.50 μg/L for the fluorescence modality and 0.77 μg/L for the SERS modality (computed according to the IUPAC definition, LOD=3σ/s, where σ and s are the standard deviation of the blank measurements (n=12) and the slope of the calibration curve), which are both lower than the WHO-suggested provisional upper limit of 1.0 μg/L in drinking water. The simultaneous availability of two independent measurements from SERS and fluorescence allows us to compute a coefficient of variation (CV) for the dual-modal sensor. The variation of CV for the dual-modal sensor with concentration is plotted in Figure 3C along with the CV values for steady-state fluorescence and SERS intensities at each concentration. The lower CV values achieved for the dual-modal sensing compared to those obtained by individual measurements demonstrate the superior performance of the developed aptasensor. We further compared the detection performance of the developed fluorescent and SERS dual-modal aptasensor in this work with some established methods in the literature, as shown in Table 2.[44–49]The results show that the present method exhibits excellent detection performance comparable to most of the listed methods; several methods show better detection performance than our current one, but these methods are very complicated, require professional expertise and long processing time, making them unsuitable for field applications. Also, the combined dual-modal detection in this work takes advantage of both fluorescence and SERS detection methods to obtain lower CV values. Together, these findings highlight the promising performance of our aptasensor for quantitative detection of MC-LR using fluorescence as well as SERS measurements.

The specificity is further explored by testing the response of this aptasensor to the analogues of MC-LR, including MC-RR and MC-YR, which are similar in molecular structure except for one functional group (Figure 4A). As expected, upon exposure to 100 μg/L MC-RR or MC-YR, the present aptasensor produces negligible changes in both fluorescence and SERS intensity even at a concentration five times higher than that of MC-LR (Figure 4B, C). The rationale is that the aptamer is highly specific toward the MC-LR through the specific

recognition of the Arg and Leu components of MC-LR. The substitution of a single Tyr in MC-YR or Arg in MC-RR for Leu disables their specific interactions with the aptamer. As a result, both MC-YR and MC-RR are unable to trigger the dissociation of aptamer from the cDNA/aptamer duplexes. Thus, we confirm that the present aptasensor exhibits excellent specificity toward MC-LR and that its structural analogues do not interfere with the fluorescence and SERS measurements. Furthermore, we use the present dual-modal aptasensor to detect MC-LR levels in three different real water samples – tap, lake, and river water samples spiked with different concentrations of MC-LR and compare the results with those obtained from the commercial ELISA kit measurements (Table 3 and Figure S7). The real water samples were prepared by spiking the tap, lake, and river water samples with stock solution of MC-LR. We find that both original tap water and original river water does not show detectable MC-LR but the original lake water has a MC-LR concentration of 1.82 μg/L, when no additional MC-LR is added. Our results show that the MC-LR concentrations obtained from the present aptasensor in either FL or SERS modality are comparable to those from the commercial ELISA test. The recovery percentage is also calculated as $(C_2\text{-}C_0)/C_1\times100\%$, where C_0, C_1 and C_2 are the concentration in the original real water, the nominal spiking concentration in the spiked real water and the concentration determined by the present aptasensor for the real water samples, respectively. As shown in Table 3, high recovery percentages and low relative standard deviation are obtained, indicating negligible interference from all three real water matrices on the developed aptasensor. Thus, these results show good accuracy and reproducibility of the present dual-modal aptasensor for detection of MC-LR in diverse environments.

In the present fluorescent-SERS dual-modal aptasensor, the plasmonic GNSs serve as the fluorescence quencher and SERS amplifier while the MC-LR specific aptamer serves as the bioreceptor. Compared to antibodies, aptamers offer higher affinity, specificity, and stability under robust conditions at low cost. Aptamers used in this work selectively bind to the Leu and Arg positions of MC-LR with high affinity and contribute to a highly specific response, as confirmed through our measurements with its analogues. In addition to its real-time nature, the measurements in this pilot study validate the sensitivity, specificity as well as the operational simplicity of this fluorescent-SERS dual-modality sensor. Furthermore, we demonstrate the applicability of the present aptasensor for the detection of MC-LR in diverse environments.

CONCLUSIONS

In summary, we present a sensitive and selective aptasensor for fluorescent-SERS dual-modal detection of MC-LR toxins in aquatic settings. In this design, we employed the differential affinity of the Cy3-cDNA and Cy3-cDNA/aptamer duplex with the GNS to induce simultaneous, but opposite, changes of both fluorescence and SERS intensities. As a result, while strong fluorescence emission and weak SERS enhancement take place in the absence of MC-LR, appreciable fluorescence quenching and SERS enhancement were observed in the presence of the target analytes. The addition of MC-LR induces the dissociation of aptamer from the Cy3-cDNA/aptamer duplexes, and thus the single-stranded Cy3-cDNA coils around the GNS surface due to their strong binding interactions. The high affinity of the aptamer toward MC-LR endows this detection scheme with extraordinary

selectivity. The design strategy used in this work enables dual-modality quantitative detection via simultaneous measurements of fluorescence and SERS, and allows us to achieve higher precision than either fluorescence or SERS measurements alone. This method maintains high accuracy but eliminates the need for binding and washing steps of a substrate-based assay enabling the further development of a field-deployable MC-LR sensor.

EXPERIMENTAL SECTION

Materials.

Chloroauric acid ($HAuCl_4 \cdot xH_2O$, 99.999% trace metals basis), sodium citrate ($HOC(COONa)(CH_2COONa)_2 \cdot 2H_2O$, ≥99%), poly(vinylpyrrolidone) (PVP, $(C_6H_9NO)_n$, molecular weight - 10 kg/mol), $NaBH_4$ (≥99%), *N,N*-dimethylformamide (DMF, anhydrous 99.8%), tris-(2-carboxyethyl)phosphine hydrochloride (TCEP), acetate buffer (pH 5.2), Tris acetate buffer, NaCl aq. (5 M), microcystin-LR (MC-LR), microcystin-RR (MC-RR) and microcystin-YR (MC-YR) were purchased from Sigma-Aldrich (St. Louis, MO). Both Cy3-modfiied single-stranded complementary DNA (Cy3-cDNA) and MC-LR specific aptamer with sequences of 5'-Cy3-AAT GAG GTG GTA TGG GTA ATT GTC ATG GTG GTC CTG TTT G-$(CH_2)_3SS(CH_2)_3$-OH-3' and 5'-GGC GCC AAA CAG GAC CAC CAT GAC AAT TAC CCA TAC CAC CTC ATT ATG CCC CAT CTC CGC-3' were ordered from Integrated DNA Technologies (IDT, Coralville, IA).[39] The commercial MC-LR ELISA kit was ordered from Shanghai Xin Yu Biotech Co., Ltd (Shanghai, China). All other reagents and solvents were of analytical grade and used as received.

Instrumentation and characterization.

Both absorption spectra and melting point measurements were taken using an Aviv Model 14DS UV-vis spectrophotometer (Aviv Biomedical, Lakewood, NJ). Both fluorescence emission spectra and time-dependent profiles of fluorescence intensity at 565 nm were collected on an Aviv ATF 105 Spectrofluorimeter (Aviv Biomedical, Lakewood, NJ) with the excitation of 510 nm. Transmission electron microscopic (TEM) images were obtained on an FEI Tecnai T12 microscope (FEI, Hillsboro, OR) at an accelerating voltage 120 kV. The air-dried samples were prepared through deposition of a drop of samples onto the TEM 200-mesh copper grid (Ted Pella, Redding, CA). The ELISA measurements were performed on a TECAN Spark microplate reader (Tecan, Switzerland). Both spontaneous Raman and SERS measurements were conducted using a home-built, inverted high-speed Raman confocal microscope equipped with a compact LM series volume holographic grating-stabilized 785 nm near-infrared diode laser, a 60× oil immersion Olympus objective lens (0.65–1.25 NA), a HoloSpec f/1.8 spectrograph and an iDus CCD camera. The detailed information related to the set-up can be found in our previous work.[37,50] The SERS measurements were acquired at room temperature with 1 s integration time and a laser power of 5 mW at the sample, unless otherwise mentioned. The SERS spectra were presented with the background subtracted using a polynomial fitting of fifth order.[51,52]

Synthesis of gold nanostars.

GNSs were synthesized by the seed-mediated growth method well-established in our previous work.[37] The gold seed solution was first prepared by reducing $HAuCl_4$ with

sodium citrate and $NaBH_4$. 1 mL of $HAuCl_4$ (1 wt%) aqueous solution was diluted to 90 mL with deionized water followed by the addition of 2 mL 38.8 mM sodium citrate aqueous solution. Then, 1 mL of freshly prepared $NaBH_4$ solution (0.075 wt% in 38.8 mM sodium citrate aqueous solution) was slowly added. The reaction was kept at room temperature overnight, finally producing a gold seed solution with wine-red color. 50 mL of the gold seed solution was added with PVP (10 mM) at room temperature followed by constant stirring for 24 h to obtain the PVP-coated gold seed solution. Following this, 82 μL of 50 mM $HAuCl_4$ aqueous solution was added to 15 mL DMF containing 10 mM PVP, and then 86 μL of PVP-coated gold seed solution was rapidly added with constant stirring at room temperature for 3 h. The extinction spectrum shows no change when the growth time exceeds 30 min, indicating that the growth of GNS is completed within 30 min. The resulting GNSs were successively centrifuged at 11000 rpm for 15 min and washed at least three times with ethanol, and after annealing at 90 ^{o}C for 30 min, GNSs were dissolved in deionized water to get a concentration of 0.5 nM for further use.

Preparation of Cy3-cDNA-GNS conjugates.

Glass vials were soaked in a 12 M NaOH aqueous solution for 1 h and rinsed with DI water before use. 9 μL of 1 mM Cy3-cDNA was added into a microcentrifuge tube containing 1 μL 500 mM acetate buffer solution (pH 5.2). Then, 2 μL of 10 mM TCEP was added followed by incubation at room temperature for 1 h to reduce and activate the thiol-modified Cy3-cDNA. 3 mL DI water was added and the UV-vis absorption measurement was performed to quantify the Cy3-cDNA amount. 240 μL of 0.5 nM GNS aqueous solutions was added to the TCEP-treated Cy3-cDNA solution with gentle shaking by hand, and incubated for at least 16 h in the dark. 20 μL of 1 M NaCl aqueous solution was added every three hours to get a final NaCl concentration of 100 mM. The solution was centrifuged and washed at least three times with a solution containing 100 mM NaCl and 25 mM Tris acetate (pH 8.2). The Cy3-cDNA-GNS conjugates were dissolved in the Tri acetate buffer solution (25 mM) containing 50 mM NaCl, to reach a concentration of 40 pM for further use. The supernatant was examined by the UV-vis absorption measurement. The Cy3-cDNA coverage was calculated to be 4862 cDNA strand per GNS nanoparticle.

Preparation of Cy3-cDNA/aptamer-GNS conjugates and melting point measurement.

To form the Cy3-cDNA/aptamer duplex on GNSs, the aptamer stock solution (1 mM) was added at a final concentration of 510 nM, and then incubated overnight at 4^{o}C. The excess aptamer was removed by centrifugation at 11000 rpm and the precipitates were re-dispersed in 25 mM Tris acetate buffer solution containing various NaCl concentrations (50, 100 and 150 mM). Such a solution can be used for melting point measurement and detection of microcystins.

For melting point measurements, the absorbance at 260 nm was recorded at a rate of 0.5 ^{o}C/min in 2 ^{o}C intervals in the 4^{o}C-90^{o}C temperature range, and the equilibrium time is set to 1 min before each test. Samples were magnetically stirred during the melting point test to preclude the effect of precipitation. The melting point was determined by taking the first derivative of the melting curves.

Preparation of real water samples.

Tap water, lake water and river water samples were collected from the university laboratory tap, Dongting Lake and Xiang River (Hunan, China). All real water samples were centrifuged at 4000 rpm for 10 min at least three times and supernatants were collected as original real water samples. The MC-LR concentrations in original tap water, lake water and river water were analysed by the commercial ELISA kit according to the manufacturer's instructions. The stock solution of MC-LR was spiked into original water samples of tap water, lake water and river water to obtain their final concentrations of MC-LR, respectively.

Detection of microcystins.

Detection of MC-LR is based on the MC-LR-aptamer interaction, resulting in the dissociation of the Cy3-cDNA/aptamer duplex and the concomitant changes of fluorescence and SERS intensity. The solutions of Cy3-cDNA/aptamer-GNS conjugates (40 pM) in the Tri acetate buffer solution obtained above were spiked with various MC-LR concentrations (0, 0.1, 0.5, 1.0, 5.0, 10, 20, and 50 μg/L), which were subject to both fluorescence and SERS measurements. The fluorescence measurements were performed with solutions in a quartz cuvette with the excitation wavelength of 510 nm. The SERS spectra were collected in 2.5 μL of the solutions aforementioned with 1 s integration time and a laser power of 5 mW at the sample. At least twenty SERS spectra were acquired at each measurement and the averaged spectra were presented. The MC-LR's analogues, MC-RR and MC-YR, were employed as control to examine the selectivity of the present fluorescent-SERS dual-modal aptasensor. All measurements were performed in triplicate.

Numerical Simulations.

Finite-difference time-domain (FDTD) simulation was conducted using the commercial software Lumerical FDTD Solutions 8.6 (Lumerical Solutions Inc., Vancouver, Canada) to observe the electric field distribution at 785 nm of the GNS. The geometric model was created according to the structure shown in the TEM data. The dielectric function of gold was taken from the experimental data tabulated by Johnson and Christy.[53] Water with a refractive index of 1.33 was used as the background. The mesh size of the box containing the GNS and its surrounding space was 0.5 nm. A total-field scattered-field was used as the input source. The geometric model for the FDTD simulations was verified by the consistence of the calculated LSPR wavelength with the experimental plasmonic resonance wavelength.

Supplementary Material

Refer to Web version on PubMed Central for supplementary material.

Funding

This research was supported by National Natural Science Foundation of China (No. 51871246), Hunan Provincial Science & Technology Program (No. 2017XK2027) and JHU Water Institute Seed Grant. This research was also partially supported by the JHU Whiting School of Engineering Seed Funds. I. B. acknowledges the support from the National Institute of Biomedical Imaging and Bioengineering (2-P41-EB015871-31) and National Institute of General Medical Sciences (DP2GM128198).

References:

(1). Yager P; Domingo GJ; Gerdes J Point-of-care Diagnostics for Global Health. Annu. Rev. Biomed. Eng 2008, 10, 107–44. [PubMed: 18358075]

(2). Shepherd R; Beirne S; Lau KT; Corcoran B; Diamond D Monitoring Chemical Plumes in an Environmental Sensing Chamber with a Wireless Chemical Sensor Network. Sens. Actuator B-Chem 2007, 121, 142–149.

(3). Zhang W; Asiri AM; Liu D; Du D; Lin Y Nanomaterial-based Biosensors for Environmental and Biological Monitoring of Organophosphorus Pesticides and Nerve Agents. Trends Anal. Chem 2014, 54, 1–10.

(4). Xing C; Liu L; Song S; Feng M; Kuang H; Xu C Ultrasensitive Immunochromatographic Assay for the Simultaneous Detection of Five Chemicals in Drinking Water. Biosens. Bioelectron 2015, 66, 445–453. [PubMed: 25499659]

(5). Liu L; Xing C; Yan H; Kuang H; Xu C Development of an ELISA and Immunochromatographic Strip for Highly Sensitive Detection of Microcystin-LR. Sensors 2014, 14(8), 14672–14685. [PubMed: 25120158]

(6). Kong D; Xie Z; Liu L; Song S; Kuang H; Cui G; Xu C Development of Indirect Competitive ELISA and Lateral-flow Immunochromatographic Assay Strip for the Detection of Sterigmatocystin in Cereal Products. Food Agric. Immunol 2017, 28(2), 260–273.

(7). Kong D; Liu L; Song S; Suryoprabowo S; Li A; Kuang H; Wang L; Xu C A Gold Nanoparticle-based Semi-quantitative and Quantitative Ultrasensitive Paper Sensor for the Detection of Twenty Mycotoxins. Nanoscale 2016, 8(9), 5245–5253. [PubMed: 26879591]

(8). Fan W; Yung B; Huang P; Chen X Nanotechnology for Multimodal Synergistic Cancer Therapy. Chem. Rev 2017, 117, 13566–13638. [PubMed: 29048884]

(9). Shan B; Pu Y; Chen Y; Liao M; Li M Novel SERS Labels: Rational Design, Functional Integration and Biomedical Applications. Coord. Chem. Rev 2018, 371, 11–37.

(10). Qian X; Peng XH; Ansari DO; Yin-Goen Q; Chen GZ; Shin DM; Yang L; Young AN; Wang MD; Nie S In vivo Tumor Targeting and Spectroscopic Detection with Surface-enhanced Raman Nanoparticle Tags. Nat. Biotechnol 2008, 26, 83–90. [PubMed: 18157119]

(11). Sugawa K; Tamura T; Tahara H; Yamaguchi D; Akiyama T; Otsuki J; Kusaka Y; Fukuda N; Ushijima H Metal-enhanced Fluorescence Platforms Based on Plasmonic Ordered Copper Arrays: Wavelength Dependence of Quenching and Enhancement Effects. ACS Nano 2013, 7, 9997–10010. [PubMed: 24090528]

(12). Ali MR; Wu Y; Han T; Zang X; Xiao H; Tang Y; Wu R; Fernandez FM; El-Sayed MA Simultaneous Time-Dependent Surface-Enhanced Raman Spectroscopy, Metabolomics, and Proteomics Reveal Cancer Cell Death Mechanisms Associated with Gold Nanorod Photothermal Therapy. J. Am. Chem. Soc 2016, 138, 15434–15442. [PubMed: 27809520]

(13). Kumar A; Kim S; Nam JM Plasmonically Engineered Nanoprobes for Biomedical Applications. J. Am. Chem. Soc 2016, 138, 14509–14525. [PubMed: 27723324]

(14). Li M; Wang Q; Shi X; Hornak LA; Wu N Detection of Mercury (II) by Quantum Dot/DNA/Gold Nanoparticle Ensemble Based Nanosensor via Nanometal Surface Energy Transfer. Anal. Chem 2011, 83, 7061–7065. [PubMed: 21842845]

(15). de Figueiredo DR; Azeiteiro UM; Esteves SM; Gonçalves FJ; Pereira MJ Microcystin-Producing Blooms—a Serious Global Public Health Issue. Ecotoxicol. Environ. Saf 2004, 59, 151–163. [PubMed: 15327870]

(16). World Health Organization (WHO), Cyanobacterial Toxins: Microcystin-LR in Drinking-Water Background Document for Development of WHO Guidelines for Drinking-water Quality. Geneva, Switzerland World Health Organization, 2nd ed Geneva, 2003.

(17). Wu S; Duan N; Zhang H; Wang Z Simultaneous Detection of Microcysin-LR and Okadaic Acid Using a Dual Fluorescence Resonance Energy Transfer Aptasensor. Anal. Bioanal. Chem 2015, 407, 1303–1312. [PubMed: 25492092]

(18). Zrimsek AB; Chiang N; Mattei M; Zaleski S; McAnally MO; Chapman CT; Henry AI; Schatz GC; Van Duyne RP Single-Molecule Chemistry with Surface-and Tip-Enhanced Raman Spectroscopy. Chem. Rev 2016, 11, 7583–7613.

(19). Chen C; Midelet C; Bhuckory S; Hildebrandt N; Werts MH Nanosurface Energy Transfer from Long-lifetime Terbium Donors to Gold Nanoparticles. J. Phys. Chem. C 2018, 122, 17566–17574.

(20). Li M; Cushing SK; Wang Q; Shi X; Hornak LA; Hong Z; Wu N Size-dependent Energy Transfer Between CdSe/ZnS Quantum Dots and Gold Nanoparticles. J. Phys. Chem. Lett 2011, 2, 2125–2129.

(21). Jin Y; Gao X Plasmonic Fluorescent Quantum Dots. Nat. Nanotechnol 2009, 4, 571–576. [PubMed: 19734929]

(22). Smith BR; Gambhir SS Nanomaterials for In Vivo Imaging. Chem. Rev 2017, 117, 901–986 [PubMed: 28045253]

(23). Zavaleta CL; Smith BR; Walton I; Doering W; Davis G; Shojaei B; Natan MJ;Gambhir SS Multiplexed Imaging of Surface Enhanced Raman Scattering Nanotags in Living Mice Using Noninvasive Raman Spectroscopy. Proc. Natl. Acad. Sci. U.S.A 2009, 106, 13511–13516. [PubMed: 19666578]

(24). Dick S; Konrad MP; Lee WW; McCabe H; McCracken JN; Rahman T; Stewart A; Xu Y; Bell SE Surface-Enhanced Raman Spectroscopy as a Probe of the Surface Chemistry of Nanostructured Materials. Adv. Mater 2016, 28, 5705–5711. [PubMed: 26822589]

(25). Zong S; Chen C; Wang Z; Zhang Y; Cui Y Surface Enhanced Raman Scattering Based in Situ Hybridization Strategy for Telomere Length Assessment. ACS Nano 2016, 10, 2950–2959. [PubMed: 26812475]

(26). Aioub M; El-Sayed MA A Real-Time Surface Enhanced Raman Spectroscopy Study of Plasmonic Photothermal Cell Death Using Targeted Gold Nanoparticles. J. Am. Chem. Soc 2016, 138, 1258–1264. [PubMed: 26746480]

(27). Lane LA; Qian X; Nie S SERS Nanoparticles in Medicine: from Label-free Detection to Spectroscopic Tagging. Chem. Rev 2015, 115, 10489–10529. [PubMed: 26313254]

(28). Yue S; Sun X; Wang N; Wang Y; Wang Y; Xu Z; Chen M; Wang J SERS–Fluorescence Dual-Mode pH-Sensing Method Based on Janus Microparticles. ACS Appl. Mater. Interfaces 2017, 9, 39699–39707. [PubMed: 29063750]

(29). Lee S; Chon H; Yoon SY; Lee EK; Chang SI; Lim DW; Choo J Fabrication of SERS-Fluorescence Dual Modal Nanoprobes and Application to Multiplex Cancer Cell Imaging. Nanoscale 2012, 4, 124–129. [PubMed: 22080302]

(30). Gabudean AM; Focsan M; Astilean S Gold Nanorods Performing as Dual-modal Nanoprobes via Metal-enhanced Fluorescence (MEF) and Surface-enhanced Raman Scattering (SERS). J. Phys. Chem. C 2012, 116, 12240–12249.

(31). He D; Wu Z; Cui B; Jin Z A Novel SERS-based Aptasensor for Ultrasensitive Sensing of Microcystin-LR. Food Chem. 2019, 278, 197–202. [PubMed: 30583362]

(32). Zhao Y; Yang X; Li H; Luo Y; Yu R; Zhang L; Yang Y; Song Q Au Nanoflower–Ag Nanoparticle Assembled SERS-active Substrates for Sensitive MC-LR Detection. Chem. Commun 2015, 51(95), 16908–16911.

(33). Bostan HB; Taghdisi SM; Bowen JL; Demertzis N; Rezaee R; Panahi Y; Tsatsakis AM; Karimi G Determination of Microcystin-LR, Employing Aptasensors. Biosens. Bioelectron 2018, 119, 110–118. [PubMed: 30121422]

(34). He S; Xie W; Fang S; Zhou D; Djebbi K; Zhang Z; Du J; Du C; Wang D Label-free Identification of Trace Microcystin-LR with Surface-enhanced Raman Scattering Spectra. Talanta 2019, 195, 401–406. [PubMed: 30625561]

(35). Li H; Rothberg L Colorimetric Detection of DNA Sequences Based on Electrostatic Interactions with Unmodified Gold Nanoparticles. Proc. Natl. Acad. Sci. U.S.A 2004, 101, 14036–14039. [PubMed: 15381774]

(36). Nelson EM; Rothberg LJ Kinetics and Mechanism of Single-Stranded DNA Adsorption onto Citrate-Stabilized Gold Nanoparticles in Colloidal Solution. Langmuir 2011, 27, 1770–1777. [PubMed: 21218826]

(37). Li M; Kang JW; Dasari RR; Barman I Shedding Light on the Extinction-Enhancement Duality in Gold Nanostar-Enhanced Raman Spectroscopy. Angew. Chem. Int. Ed 2014, 53, 14115–14119.

(38). Li M; Cushing SK; Zhang J; Lankford J; Aguilar ZP; Ma D; Wu N Shape-dependent Surface-Enhanced Raman Scattering in Gold–Raman-Probe–Silica Sandwiched Nanoparticles for Biocompatible Applications. Nanotechnology 2012, 23, 115501. [PubMed: 22383452]

(39). Ng A; Chinnappan R; Eissa S; Liu H; Tlili C; Zourob M Selection, Characterization, and Biosensing Application of High Affinity Congener-Specific Microcystin-Targeting Aptamers. Environ. Sci. Technol 2012, 46, 10697–10703. [PubMed: 22958101]

(40). Liu J; Lu Y Preparation of Aptamer-linked Gold Nanoparticle Purple Aggregates for Colorimetric Sensing of Analytes. Nat. Protoc 2006, 1, 246–252. [PubMed: 17406240]

(41). Feng AL; You ML; Tian L; Singamaneni S; Liu M; Duan Z; Lu TJ; Xu F; Lin M Distance-dependent Plasmon-enhanced Fluorescence of Upconversion Nanoparticles Using Polyelectrolyte Multilayers as Tunable Spacers. Sci. Rep 2015, 5, 7779. [PubMed: 25586238]

(42). Shi H; Chen N; Su Y; Wang H; He Y Reusable Silicon-based Surface-enhanced Raman Scattering Ratiometric Aptasensor with High Sensitivity, Specificity, and Reproducibility. Anal. Chem 2017, 89(19), 10279–10285. [PubMed: 28882037]

(43). Simoncelli S; Roller EM; Urban P; Schreiber R; Turberfield AJ; Liedl T; Lohmüller T Quantitative Single-molecule Surface-enhanced Raman Scattering by Optothermal Tuning of DNA Origami-assembled Plasmonic Nanoantennas. ACS Nano 2016, 10(11), 9809–9815. [PubMed: 27649370]

(44). Chen K; Liu M; Zhao G; Shi H; Fan L; Zhao S Fabrication of a Novel and Simple Microcystin-LR Photoelectrochemical Sensor with High Sensitivity and Selectivity. Environ. Sci. Technol 2012, 46(21), 11955–11961. [PubMed: 23030666]

(45). Zhu Y; Kuang H; Xu L; Ma W; Peng C; Hua Y; Wang L; Xu C Gold Nanorod Assembly Based Approach to Toxin Detection by SERS. J. Mater. Chem 2012, 22(6), 2387–2391.

(46). Wang L; Chen W; Xu D; Shim BS; Zhu Y; Sun F; Liu L; Peng C; Jin Z; Xu C; Kotov NA Simple, Rapid, Sensitive, and Versatile SWNT–paper Sensor for Environmental Toxin Detection Competitive with ELISA. Nano Lett. 2009, 9(12), 4147–4152. [PubMed: 19928776]

(47). Li M; Paidi SK; Sakowski E; Preheim SP; Barman I Ultrasensitive Detection of Hepatotoxic Microcystin Production from Cyanobacteria Using Surface–enhanced Raman Scattering (SERS) Immunosensor. ACS Sens. 2019, 4, 1203–1210. [PubMed: 30990314]

(48). Li Y; Sun J; Wu L; Ji J; Sun X; Qian Y Surface-enhanced Fluorescence Immunosensor Using Au Nano-crosses for the Detection of Microcystin-LR. Biosens. Bioelectron 2014, 62, 255–260. [PubMed: 25016333]

(49). Reverté L; Garibo D; Flores C; Diogène J; Caixach J; Campàs M Magnetic Particle-Based Enzyme Assays and Immunoassays for Microcystins: from Colorimetric to Electrochemical Detection. Environ. Sci. Technol 2012, 47(1), 471–478.

(50). Li M; Kang JW; Sukumar S; Dasari RR; Barman I Multiplexed Detection of Serological Cancer Markers with Plasmon-Enhanced Raman Spectro-Immunoassay. Chem. Sci 2015, 6, 3906–3914. [PubMed: 26405519]

(51). Beier BD; Berger AJ Method for Automated Background Subtraction from Raman Spectra Containing Known Contaminants. Analyst 2009, 134(6), 1198–1202. [PubMed: 19475148]

(52). Cadusch PJ; Hlaing MM; Wade SA; McArthur SL; Stoddart PR Improved Methods for Fluorescence Background Subtraction from Raman Spectra. J. Raman Spectrosc 2013, 44(11), 1587–1595.

(53). Johnson PB; Christy RW Optical Constants of the Noble Metals. Phys. Rev. B 1972, 6, 4370.

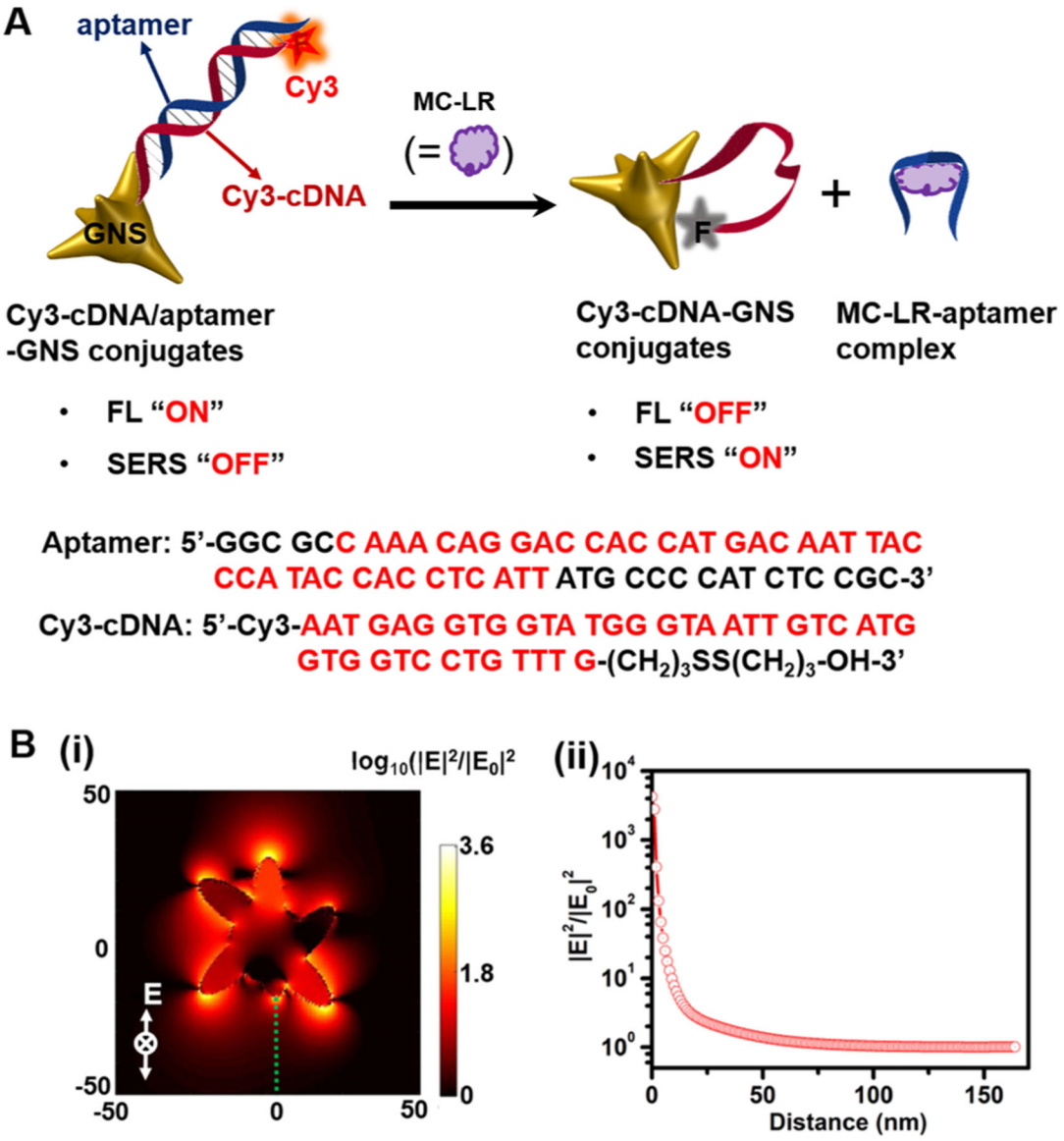

Figure 1.

(A) Schematic of the fluorescent-SERS dual-modal aptasensor for detection of MC-LR. MC-LR preferentially binds to aptamer of Cy3-cDNA/aptamer-GNS conjugates, leading to the dissociation of aptamer from and sticking of Cy3-cDNAs to the GNS surface. This enables fluorescence quenching and SERS enhancement of Cy3 dyes. Sequences of the MC-LR specific aptamers and Cy3-cDNA are also shown here. (B) (i) Calculated electric field ($|E|^2/|E_0|^2$) distribution of a single GNS excited at 785 nm; and (ii) the E-field enhancement as a function of the distance away from the GNS tip, marked with the green dot line in the panel (i).

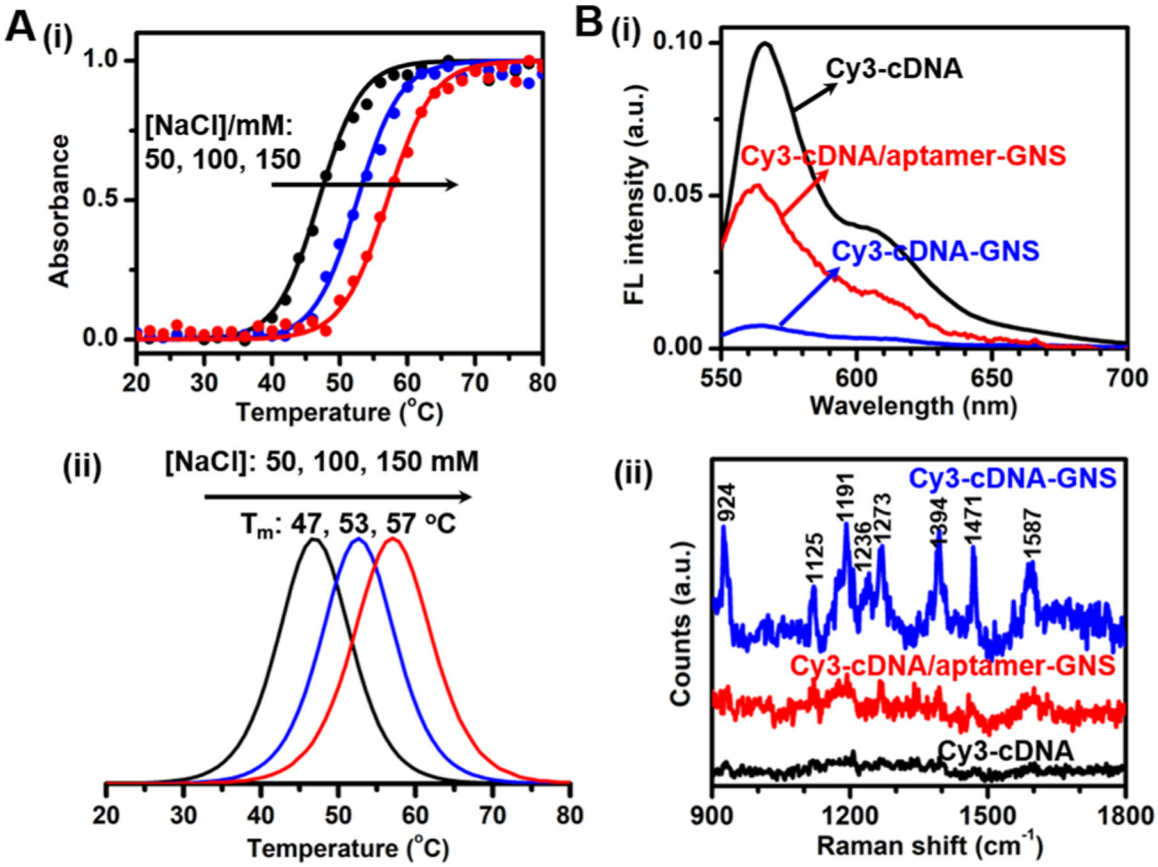

Figure 2.

(A) Melting profiles of Cy3-cDNA/aptamer-GNS conjugates in 25 mM Tris acetate buffer solutions containing 50, 100 or 150 mM NaCl. The bottom panel (ii) shows the first derivatives of the corresponding melting curves (i, top). (B) (i) Fluorescence and (ii) SERS spectra of Cy3-cDNA (black), Cy3-cDNA-GNS conjugates (blue) and Cy3-cDNA/aptamer-GNS conjugates (red). Both fluorescence and SERS spectra of Cy3-cDNA are acquired with a concentration of 3.3 μM MC-LR. Spontaneous Raman spectrum of Cy3-cDNA is measured with a 60 mW laser power and 5 s integration time, and SERS spectra of Cy3-cDNA-GNS conjugates and Cy3-cDNA/aptamer-GNS conjugates were measured with a 5 mW laser power and 1 s integration time.

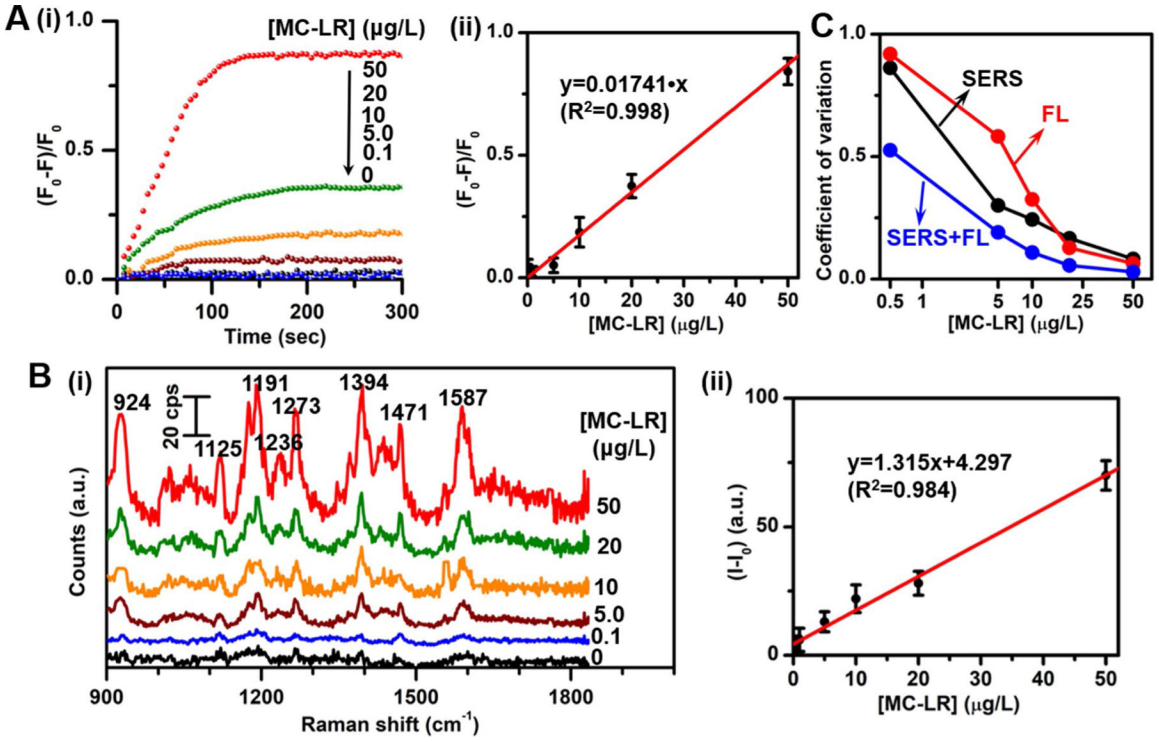

Figure 3.

(A) (i) Real-time fluorescence response ((F_0-F)/F_0) of the present aptasensor with respect to the initial (time=0) fluorescence intensity (F_0) at 565 nm and (ii) calibration curve of the relative fluorescence intensity change ((F_0-F)/F_0) at 565 nm as a function of the MC-LR concentration. (B) (i) SERS spectra and (ii) calibration curve of SERS intensity at 1394 cm $^{-1}$ as a function of the MC-LR concentration. (C) Coefficient of variation of SERS, fluorescence and the combined dual-modal detection of the present aptasensor.

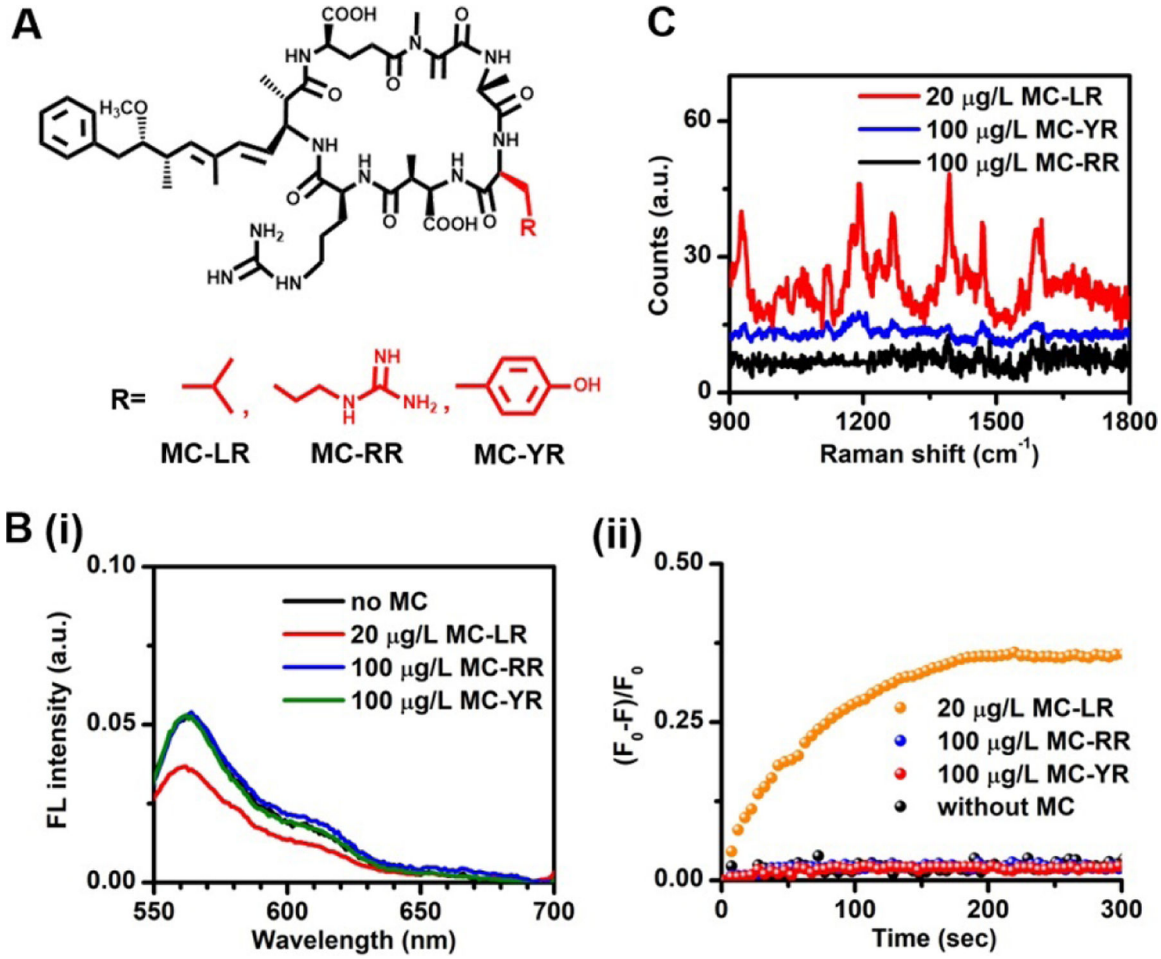

Figure 4.

(A) Molecular structures of MC-LR and its analogues, MC-RR and MC-YR. (B) (i) Steady-state fluorescence spectra and (ii) real-time fluorescence response at 565 nm of the aptasensor in the absence of microcystin as well as in the presence of 20 μg/L MC-LR, 100 μg/L MC-RR and 100 μg/L MC-YR. (C) SERS spectra of the aptasensor in the presence of 20 μg/L MC-LR, 100 μg/L MC-RR and 100 μg/L MC-YR.

Table 1.

Assignments of SERS bands of Cy3-cDNA-GNS conjugates.[42,43]

Raman shift cm^{-1}	Assignment	Raman shift cm^{-1}	Assignment
924	C-H out-of-plane bending	1273	motion of $-CH_2-$ attached to the aromatic moiety
1125	C-C stretching	1394	CH_3 symmetric deformation
1191	C-H in-plane bending	1471	C=C stretching vibration in benzene ring
1236	C-C bending	1587	C=N stretching vibration

Table 2.

Comparison of measurement results for the developed fluorescent-SERS dual-modal method with representative existing methods reported in the literature for detection of MC-LR.[44–49]

Sensing system	Method	Sensing principle	Dynamic range (μg/L)	LOD (μg/L)	Ref.
TiO_2 nanotube/molecularly imprinted polymers	PEC	current–time curve method	0.5 – 100	0.1	44
gold nanorod/antibody	SERS	SERS method	0.01 – 5.0	5.0×10^{-3}	45
carbon nanotube/porous fibrous materials	electrical	current–time curve method	0 – 10.0	0.6	46
SERS tag/antibody	SERS	SERS method	0.01 – 100	1.4×10^{-2}	47
gold nanocrosses	FL	plasmon–enhanced FL	0.02 – 16.0	7.0×10^{-3}	48
magnetic particles	ELISA	electrochemical ELISA method	0.4 – 20.0	3.9	49
Cy3/aptamer/gold nanostar	FL-SERS	FL and SERS	0.1 – 50.0	0.50 for FL 0.77 for SERS	This work

Note: PEC=photoelectrochemical; FL=fluorescence

Table 3.

Detection of MC-LR levels in the spiked real water samples from tap, Dongting Lake and Xiang River of Hunan province in China[a]

Water sample	Original [MC-LR], C_0 (μg/L)	Spiked [MC-LR], C_1 (μg/L)	ELISA (μg/L)	FL-SERS sensor, C_2		RSD		Recovery percentage	
				FL (μg/L)	SERS (μg/L)	FL (%)	SERS (%)	FL (%)	SERS (%)
Tap water	undetectable	2.03	2.14	2.08	2.12	5.77	9.91	102.46	104.43
Dongting Lake	1.82	5.01	6.71	6.89	6.99	3.34	6.29	99.42	102.34
Xiang River	undetectable	1.46	1.52	1.38	1.55	6.52	12.9	94.52	106.16

[a]Note: the real water samples from tap, Dongting Lake and Xiang River were made through spiking with the stock solution of MC-LR, respectively; original [MC-LR] were measured by the standard ELISA method; RSD is the relative standard deviation.